



Ludwig Maximilian University of Munich
Technical University of Munich
Munich GeoCenter

Dynamic rupture modeling of the 2017 M6.5 Botswana intraplate earthquake using SeisSol

HONGYI SU

Matriculation Number: *****

Thesis submitted to Munich GeoCenter
within the Joint International Masters' Programme in Geophysics

Supervisor: Prof. Dr. Alice-Agnes Gabriel
and Dr. Max Moorkamp

May 22, 2022

©2021 – HONGYI SU
All rights reserved.

Preface

In the eighteenth century, philosophers considered the whole of human knowledge, including science, to be their field and discussed questions such as: did the universe have a beginning? However, in the nineteenth and twentieth centuries, science became too technical and mathematical for the philosophers, or anyone else except a few specialists. Philosophers reduced the scope of their inquiries so much that Wittgenstein, the most famous philosopher of this century, said, “The sole remaining task for philosophy is the analysis of language.” What a comedown from the great tradition of philosophy from Aristotle to Kant! [1]

Stephen Hawking

ABSTRACT

In this thesis, we use *SeisSol*¹ to simulate the dynamic

Contents

Preface	ii
1 Theories on genesis of IPEs	1
1.1 IPEs - Common feature[2]	1
1.1.1 Old Rift	1
1.1.2 First Class of Models according to Talwani	1
1.1.3 Second Class of Models according to Talwani	2
1.1.4 Unified Model	2
1.1.5 Observations	2
1.2 Geological setting of the Botswana earthquake	3
1.2.1 Max [3]	3
1.3 Hypotheses on genesis of the Botswana earthquake	3
2 Methodology and Results	5
2.1 Static Analysis	5
2.1.1 Describe stress state on the fault plane	5
2.1.2 Fault geometry and model parameters	5
2.2 Method: SeisSol	6
2.2.1 Fault	6
2.2.2 Mesh	8
2.2.3 Initial stress	8
2.2.4 Rupture nucleation[4]	9
2.2.5 Material Perperties	9
2.2.6 Other dynamic rupture parameters	9
2.3 Result	10
2.3.1 Ground movement	10
2.3.2 Dynamic Rupture Process	12
2.3.3 Synthetic seismic data	14
2.3.4 Stress distribution: Autocoulomb	18
3 Discussion	19
3.1 Parameters and Sensitivity	19
3.1.1 Condition number	19
3.2 Seismic Hazard Assessment for Intraplate regions	19
3.2.1 Challenges	19
3.3 Comparison of seismicity data and geodetic data	19

Contents

4 Conclusion and Outlook	20
4.1 Law	20
4.1.1 Bath's Law	20
A Supporting Material for Chapter 1	21
A.0.1 Observations - Rotation of the regional stress field	21
A.0.2 Observations - Large uplifts were observed in the vicinity of faults from InSAR image	22
B Supporting Material for Chapter 2	23
B.0.1 Resistivity model	24
Bibliography	25
List of Figures	26
List of Tables	27
Nomenclature	29
Acknowledgements	30
Statement	31
Selbständigkeitserklärung	32

Chapter 1

Theories on genesis of IPEs

To explain the occurrence of IPEs

1.1 IPEs - Common feature[2]

1. The interaction of S_L and S_T can make detectable rotations of the latter (Over wavelengths of tens to hundreds of kilometres) from the seismicity data.
2. IPEs tend to occur within old rifts which contain LSCs
3. LSCs most favourable for stress buildup are stepover en echelon faults (largest IPEs)
4. In low tectonic strain rate regions, IPEs are associated with larger stress drop.
5. A variety of LSCs lead to no repeat earthquakes (explain the observation of "roaming earthquakes", i.e. successive earthquake occur on different structures)
6. Need for reevaluation of SHA techniques (IPEs not occur on preexisting fault, not repeat at same locations)

1.1.1 Old Rift

Seeking the mechanical cause for the genesis of the IPEs

1. Most of the seismic energy release is associated with rifts.
2. Preferential location of IPEs within rifts have a solid mechanical basis. (i.e. their location are not random)
3. Most of the larger IPEs are rift related.

1.1.2 First Class of Models according to Talwani

Untestable model

1. Localizing structures are assumed to be close to failure.
2. A small perturbation due to a regional stress source triggered the earthquake.

3. Variety source of small perturbation: (i). erosion or deposition at the surface (Haxby and Turcotte 1976, Calais et al. 2010); (ii). GIA (Stein et al. 1979, Zoback 1992); (iii). Stress transfer to the brittle upper crust (Liu and Zoback 1997; Kenner and Segall 2000; Pollitz et al. 2001; Sandiford and Egholm 2008)
4. These models do not address the basic cause for the stress buildup that brought the structures close to failure.

1.1.3 Second Class of Models according to Talwani

These models were developed on the basis of observed spatial association of IPEs with identifiable geologic features

1. Buried plutons (Long 1976)
2. Fault bends and intersections (King 1986; Talwani 1988)
3. Buried rift pillows (Zoback and Richardson 1996)
4. Restraining stepovers (the most notable LSCs) [2]

1.1.4 Unified Model

For rift-related IPEs

1. Stress buildup at suitable geological features (LSCs)
2. Uniform far field regional stress associated with plate margin forces
3. IPEs occur when the magnitude of this local stress buildup is comparable with the regional stress
4. This model explains how stresses build up on various geological features and many of their observed characteristics.

1.1.5 Observations

To understand the nature of IPEs within the framework of the unified model [2]

1. Confirmed by the smoothed World Stress Map data, in intraplate regions, long wavelength stress patterns(more than 2000km) of the maximum compressive horizontal stress orientation are altered by shorter spatial wavelength variations of less 200km. (Heidbach et al. 2010; Retiter et al. 2014;) Zoback (1992) attributed the deviation of the regional stress field is due to its interaction with some stress associated geologic features (LSCs).
2. Observed local rotations of the stress field. Talwani (2014) associated this rotation with the LSCs with spatial wavelength of tens to hundreds of kilometers. (Examples given are, 1925 St. Lawrence; 1811-1812 New Madrid) (See Supporting Material A.0.1)

3. Analyzing Chinese historical data going back to 2000 years, Liu et al. (2011, 2014) observed that large earthquakes (M 6) did not occur at previous epicentres. IPEs are non repeat earthquakes but rather “roaming”
4. Comparing geodetic observations to the expectation of the unified model - local pockets of elevated strain rates in the vicinity of LSCs. (Example M7.7 2011 Bhuj earthquake) (See Supporting Material A.0.2)

1.2 Geological setting of the Botswana earthquake

1.2.1 Max [3]

1. Weak upper mantle and weak crustal structure embedded in strong Precambrian blocks
2. Magnetotelluric data indicates Proterozoic continent accretion structure in the region.
3. MT data shows the event occurred along ancient thrust faults within the crust.
4. A weak zone in the uppermost mantle.
5. top-down extension as a response to large scale extensional force.
6. Hypocenters of seismic events in the region are located at the boundary of conductive structure.
7. Structures smaller than several kilometres are not detectable in their conductivity data.
8. conductive structure associated with the hypocentre of the main event.
9. the inferred fault plane coincides with a large deviation in the depth of the crustal conductor in the region

1.3 Hypotheses on genesis of the Botswana earthquake

Table 1.1: Purposed fault geometry by various research group

	Geophysicists	Strke [°]	Dip [°]	Rake [°]	Slip [m]	Depth [km]
8.2017	Kolawole et al.[5]	126 NW-SE	72-74 NE	-114	1.8	21-24
10.2017	Albano et al. [6]	304 NW-SE	65 NE	-131	2.7	20
7.2018	Gardonio et al. [7]	differ by 180 ¹	73 ± 4 or 17 ± 4	NA	NA	29 ± 4
1.2019	Materna et al. [8]	126 NW-SE	51 ± 30 SW	-107	0.66	23
10.2021	Mulabisana et al. [9]	315 NW-SE	45 NE	-80	0.50	22 ± 3

1. Deep Fluid from the upper mantle has triggered the event [7]
2. the cause of the earthquake was 1.8 m displacement along a NW striking and NE dipping normal fault that ruptured at 21–24 km depth. This seismic event was due to extensional reactivation of a crustal-scale Precambrian thrust splay within the Limpopo-Shashe orogenic belt that resulted from the collision of the Kaapvaal and Zimbabwe Cratons [5]
3. Our best-fit solution for the main shock is represented by a normal fault located at a depth greater than 20 km, dipping 65° northeast, with a right-lateral component, and a mean slip of 2.7 m. The retrieved fault geometry and mechanism are incompatible with the hypothetical stress perturbation caused by the anthropogenic activities performed in the area. Therefore, the 3 April 2017 Botswana earthquake can be classified as a natural intraplate earthquake [6]
4. 2.2020, Obtained 3-D crustal and upper mantle shear wave velocity model of Botswana. The 3 April 2017 central Botswana earthquake linked to the East African Rift System [10]

¹of two possible strike angles

Chapter 2

Methodology and Results

2.1 Static Analysis

2.1.1 Describe stress state on the fault plane

- Constrain stress state on the purposed fault to increase the chance of rupture. In fact, only few dynamic rupture setups are qualified for the best fitting rupture scenarios. To do such, we can save a great deal of CPU hours by avoiding a trial and error approach. [11]
- Under Andersonian faulting theory, only four parameters can fully describe stress state and relative strength of the fault, these are: 1. R_0 the initial relative prestress ratio; 2. μ the stress shape ratio; 3. γ the fluid pressure ratio; 4. SH_{max} the azimuth of maximum compressive stress.[12]
- Optimal stress parameters maximizes the R ratio across the fault, and the shear orientation **consistent with** observed ground deformation and focal mechanism [11]
-

2.1.2 Fault geometry and model parameters

- Fault location obtained from a fault trace that was estimated from the resistivity model in shallow depth, i.e. 5 km See **B.0.1**

The length of the fault trace is 108.46km, use a smoothing parameter 10^7 leads to a characteristic length of 92m.

the horizontal cell length of MT model is 2km

- Modeded fault is assumed at 5km beneath the surface because the fault has no surface expression.

The depth of the modeded fault is set to 37 km, supported by the kinematic model of Materna et al. [8] and aftershocks distributions.

In general, the depth of a fault is bounded by the end of the seismogenic zone, where ductile deformation takes over (becomes dominant).

- Rapid weakening Friction Law (FL=103), because I simulate dynamic scenarios.
- hydrostatic conditions, produces too large earthquake; The lithostatic case shows good consistence in observed results from other authors [11]
- SH_{max} values from 132° to 142° to be most realistic.[11]
- Translate 3D velocity model into 3D material properties.

2.2 Method: SeisSol

2.2.1 Fault

Geometry

Two faults system

- First fault, non-planar, strike 126, dip 74
- second fault, plane, strike 126, dip -28

Aftershocks

Use aftershocks to constrain our fault planes. In theory, aftershock locations should lie in the vicinity of reconstructed fault planes.

Most aftershocks occur on or near the main shock's fault plane, in practice, one can easily distinguish which is the fault plane and which is the auxiliary plane by looking at their locations. The fault area can also be estimated from the aftershock locations. Figure 2.1 shows the spatial distribution of the 2017 Botswana earthquake's aftershocks and the geometry of two purposed fault planes. In our opinion, the two fault planes fit quiet well with the aftershock locations, the most aftershocks locate near the fault planes. Due to the complexity of the aftershock's pattern, it is not possible to fit the aftershock locations with a single fault plane.

Most of aftershocks occur soon after the main shock, and decay quasi-hyperbolically with time. This decay relation is described by Omori's Law. It is widely accepted that the aftershock decay reflects stress readjustment following the stress changes due to the main shock. The depth of the main shock is thought to be at least 20km. Deep earthquakes usually do not obey the Omori's Law as they often have many fewer or even none detectable earthquakes, means that unlike friction sliding, the deep earthquakes resulting from phase change in mantle minerals, which could only produce slip once and cannot recur. (Stein)

The fact that large amount of aftershocks associated with the main shock at deep depth is interesting. However, due to limited time and incomplete data, we will not investigate further about the aftershocks in this thesis. more speacific

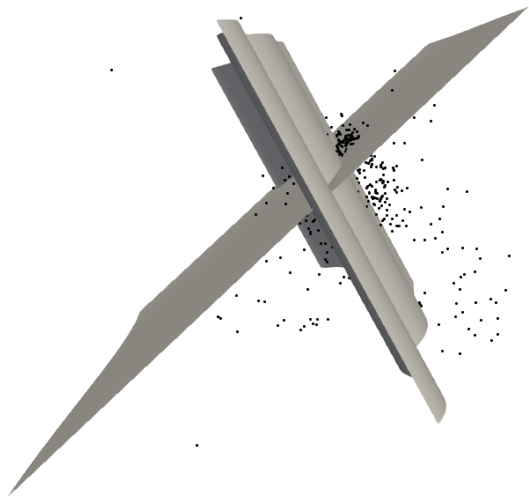


Figure 2.1: Two faults model

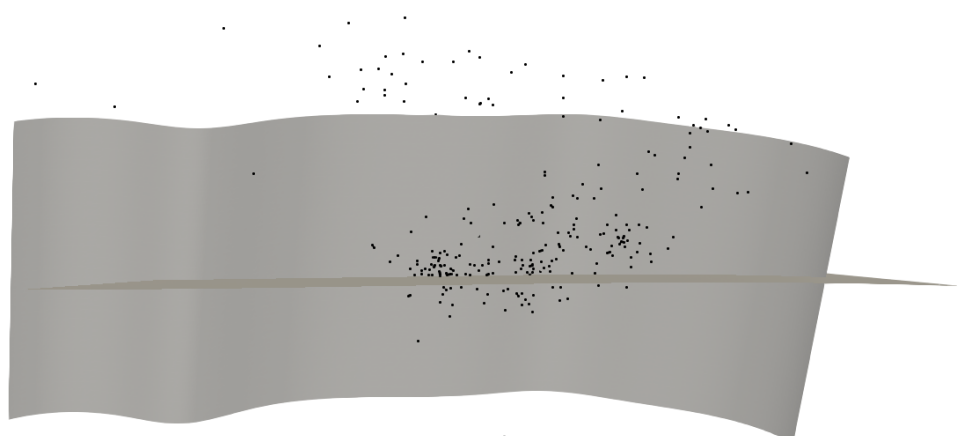


Figure 2.2: Two faults model

Published literature

Compare our purposed Two Faults model to published literature (Fadel et al. 2017) dip and strike angle...

2.2.2 Mesh

Mesh88 visualization

Figure 9 (Obermaier)

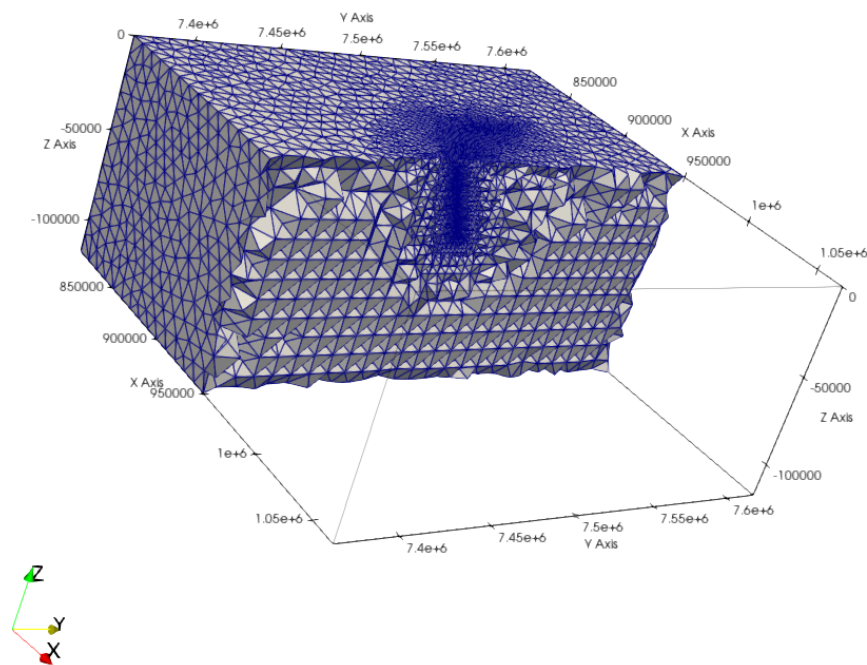


Figure 2.3: Mesh visualization

2.2.3 Initial stress

Include parameters from Static Analysis (Obermaier 2020, Gahr 2020). For example, $R = 0.7$, $SH_{max} = 132$.

2.2.4 Rupture nucleation[4]

Assuming static and dynamic friction coefficients,

$$\mu_d = 0.1 \quad (2.1)$$

$$\mu_s = 0.6 \quad (2.2)$$

and some other necessary parameters.

Rupture nucleation is caused by smoothly over stressing an area centred at the hypocenter in space and time. This can be accomplished by increasing the initial relative prestress ratio R_0 as:

$$R_{0nuc} = R_0 + F(r) \quad (2.3)$$

$$r = \sqrt{(x - x_c)^2 + (y - y_c)^2 + (z - z_c)^2} \quad (2.4)$$

where r is the nucleation radius, defined as the euclidean distance to the hypocenter (x_c, y_c, z_c) , we use $(34.404734, -18.497915, -29004.1863)$ in our simulation, that is the closest point from the fault at the depth of 29km.

$F(r)$ is a bell-shaped function:

$$F(r) = \begin{cases} \exp\left(\frac{r^2}{r^2 - r_c^2}\right), & \text{if } r < r_c. \\ 0, & \text{otherwise.} \end{cases} \quad (2.5)$$

where r_c is 1 km, represent the nucleation radius.

$$r = \sqrt{(x - x_c)^2 + (y - y_c)^2 + (z - z_c)^2} \quad (2.6)$$

2.2.5 Material Properties

RhoMuLambda.nc attached Material properties (rho, mu and lambda) translated from a regional velocity model,

$$\rho = -0.0000045 \cdot V_s^2 + 0.432 \cdot V_s + 1711 \quad (2.7)$$

2.2.6 Other dynamic rupture parameters

Adopted from Palgunadi et al. [12]

Table 2.1: SeisSol Dynamic Rupture Parameters

	Parameter	Symbol	Value
1	Direct effect parameter	a	$0.01z$
2	Evolution effect parameter	b	0.014
3	Reference slip velocity	V_0	$10^{-6}m/s$
4	Steady-state friction coefficient at V_0	f_0	0.6
5	State-evolution distance	L	0.2m
6	Weakening slip velocity	V_W	$0.1z$
7	Fully weakened friction coefficient	f_W	0.1
8	Initial slip rate	V_{ini}	$10^{-16}m/s$

2.3 Result

2.3.1 Ground movement

InSAR

High vertical deformation in the epicentral area of the Bhuj earthquake.[\[2\]](#)

Vertical deformation suggests buildup of stress at these locations, may interpret the structures where these stresses are builtup to be LSCs.[\[2\]](#)

Time: 60.000000

Obermaier (Figure 11)

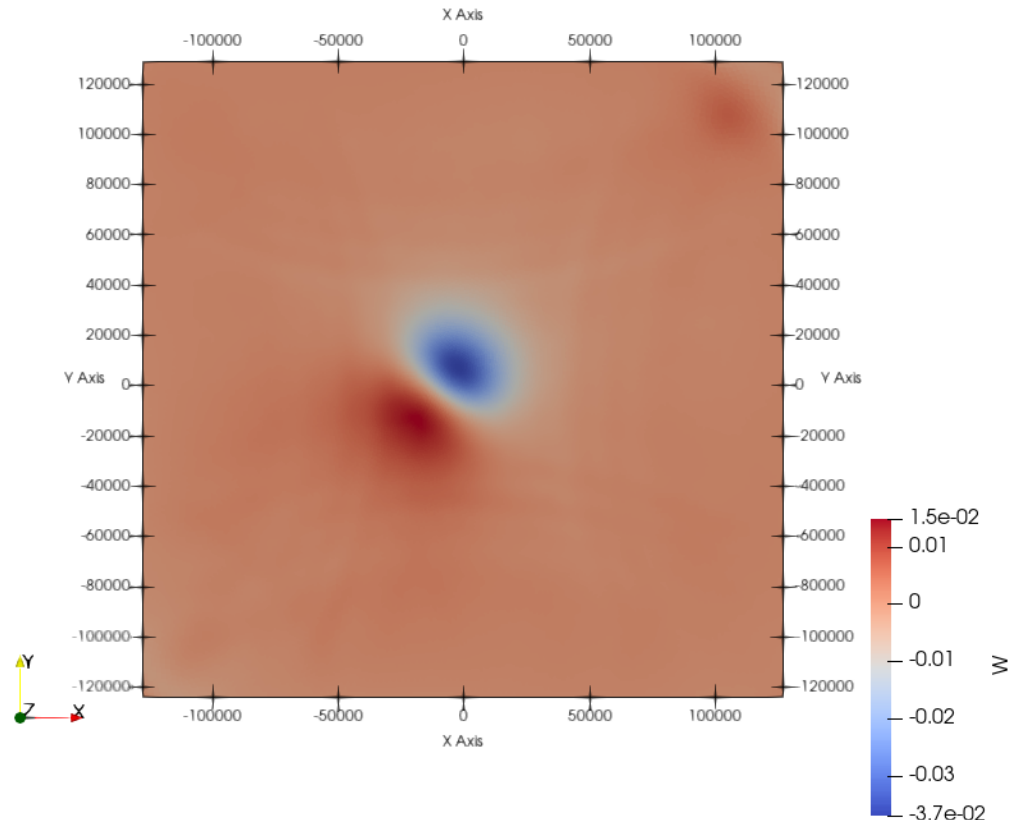


Figure 2.4: Surface displacement, vertical

Absolute Slip

The simulation shows that the absolute slip is 3.6 meters, which is unrealistic.

Chapter 2 Methodology and Results

Time: 60.000000

Obermaier (Figure 13)

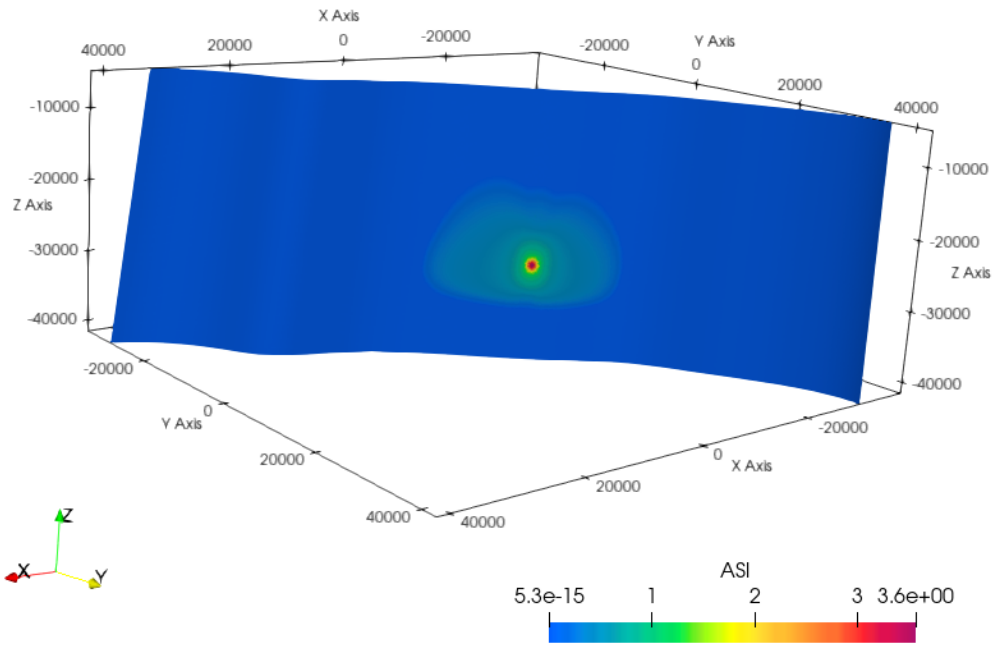
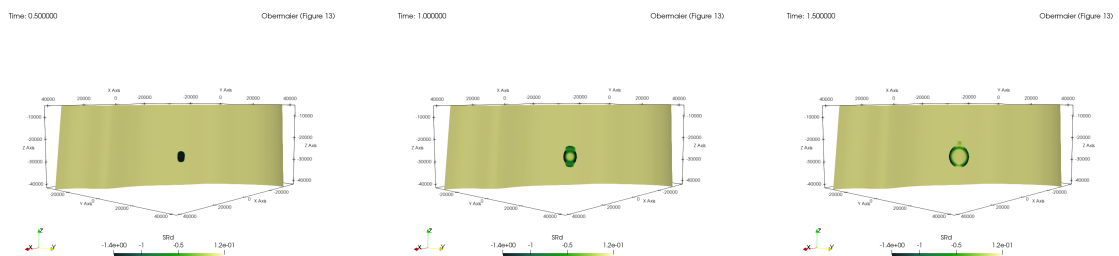


Figure 2.5: Absolute Slip

2.3.2 Dynamic Rupture Process



Chapter 2 Methodology and Results

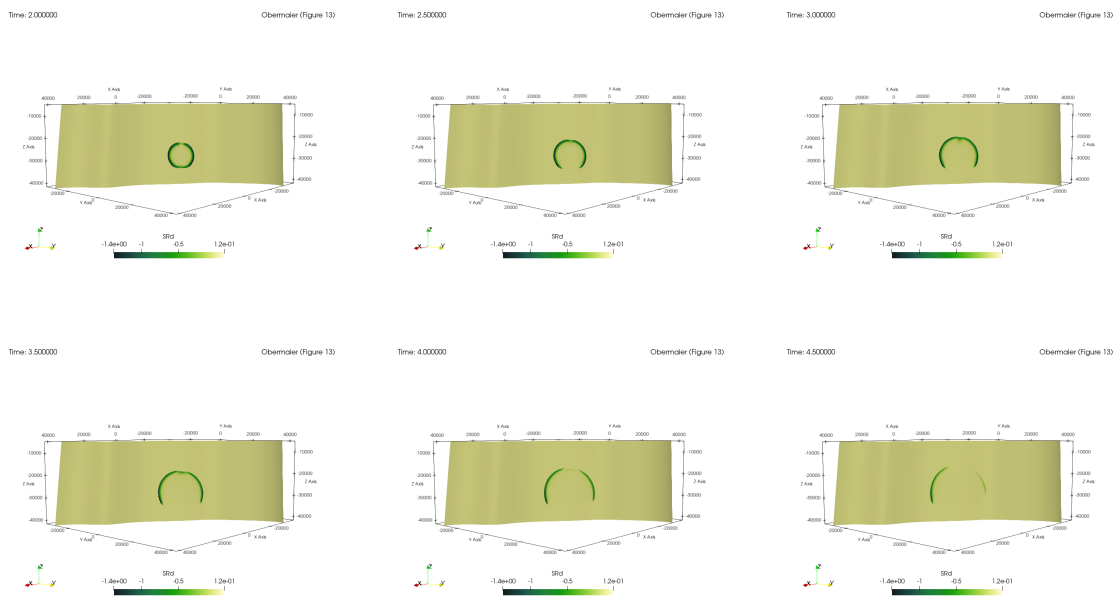


Figure 2.8: Rupture Process on the first fault plane

0.5 to 4.5 seconds out of 60.0 seconds simulation from Obermaier on the first fault plane.
SRd means slip rate in dip direction.

Chapter 2 Methodology and Results

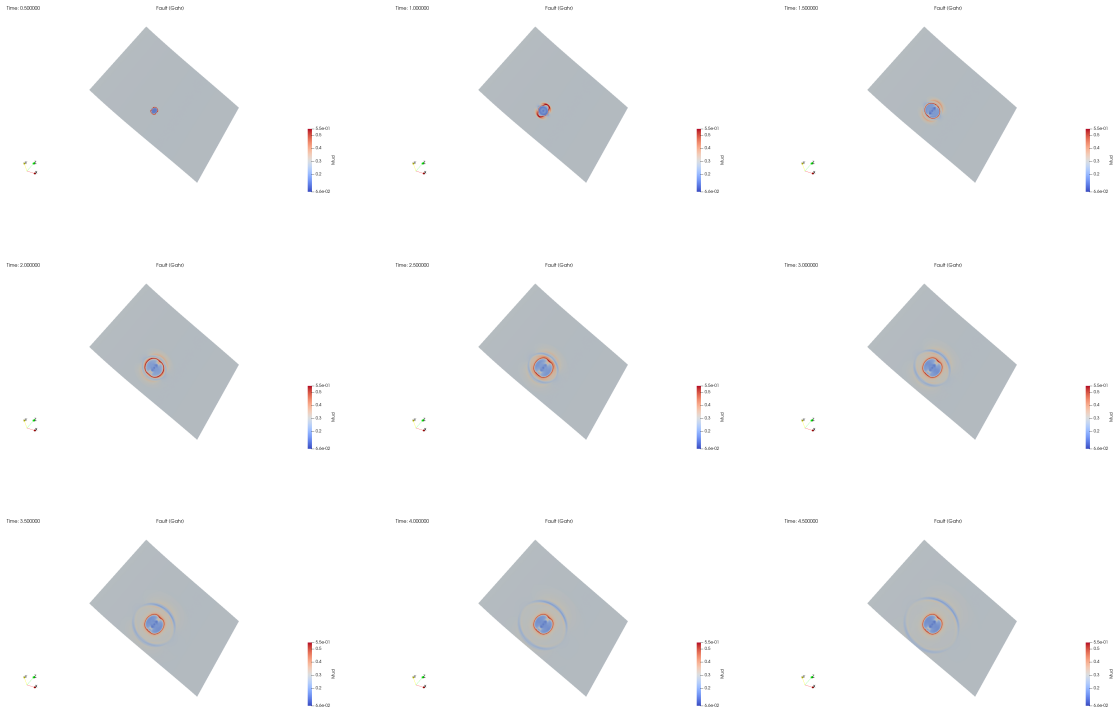


Figure 2.11: Rupture Process on the second fault plane

0.5 to 4.5 seconds out of 6.0 seconds simulation from Gahr on the second fault plane. Mud is current friction.

2.3.3 Synthetic seismic data

- Instrument correction (preprocessing) need to be done for the observational data, note that the magnitude is an order of 8 different between obs and syn;
- Need to apply a shift in time domain for observational or synthetic data in order to compare them;
- spectrum: obs scale down by 10e8

Chapter 2 Methodology and Results

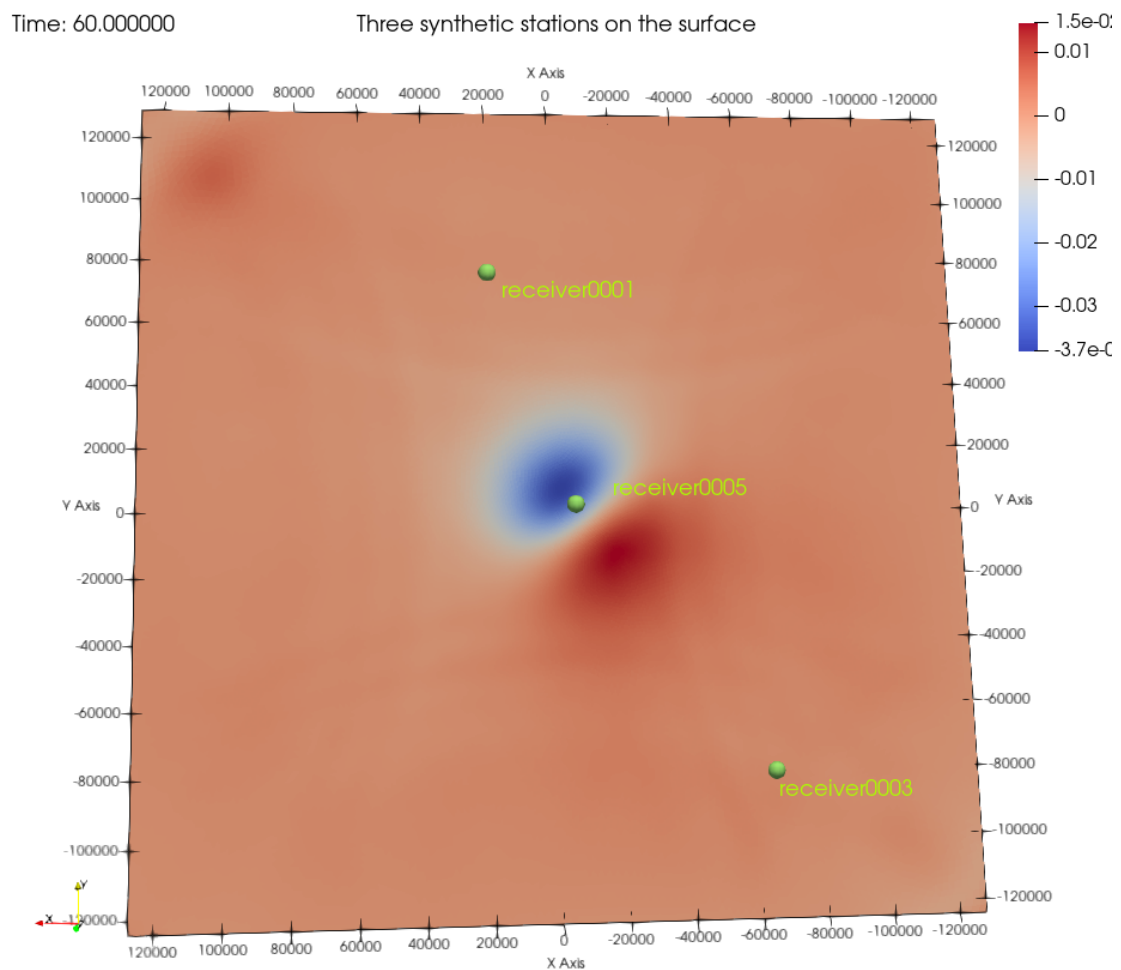


Figure 2.12: Location of the synthetic receivers

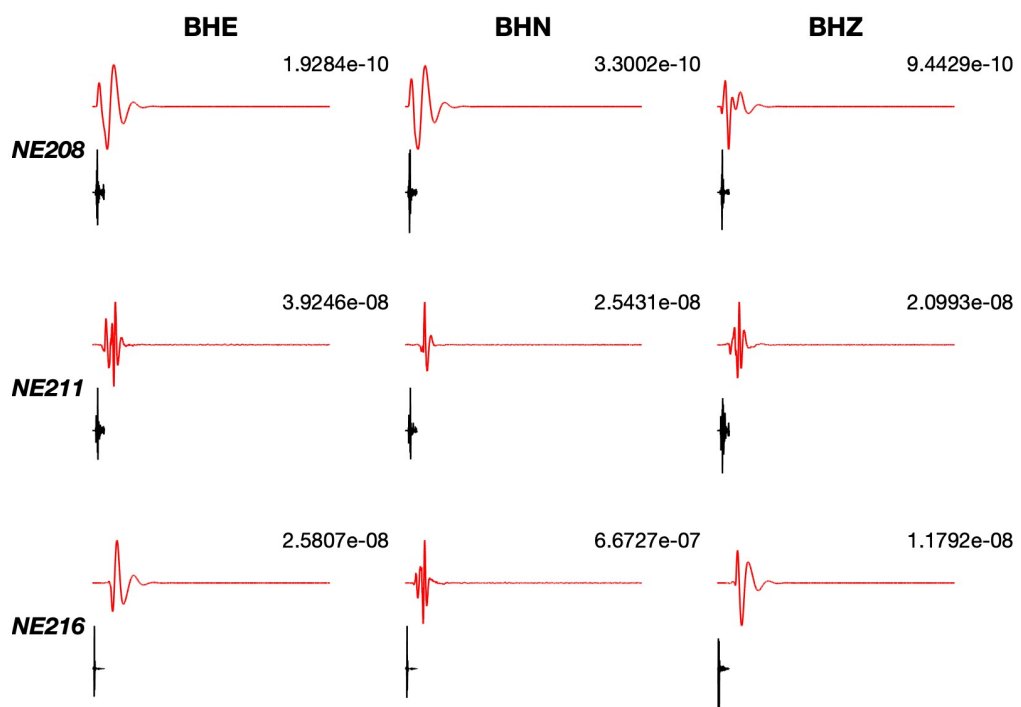


Figure 2.13: Observational and Synthetic seismogram after applied [0.2, 0.6] band pass with order 4 Butterworth filter

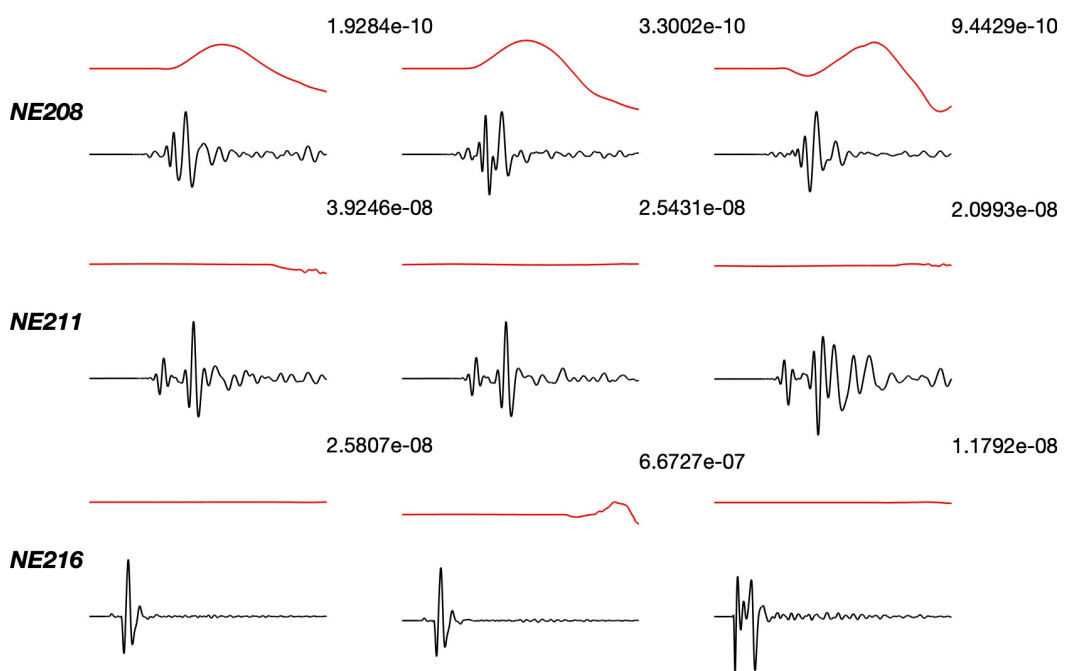


Figure 2.14: Observational and Synthetic seismogram after applied $[0.2, 0.6]$ band pass with order 4 Butterworth filter, cut in 60 seconds

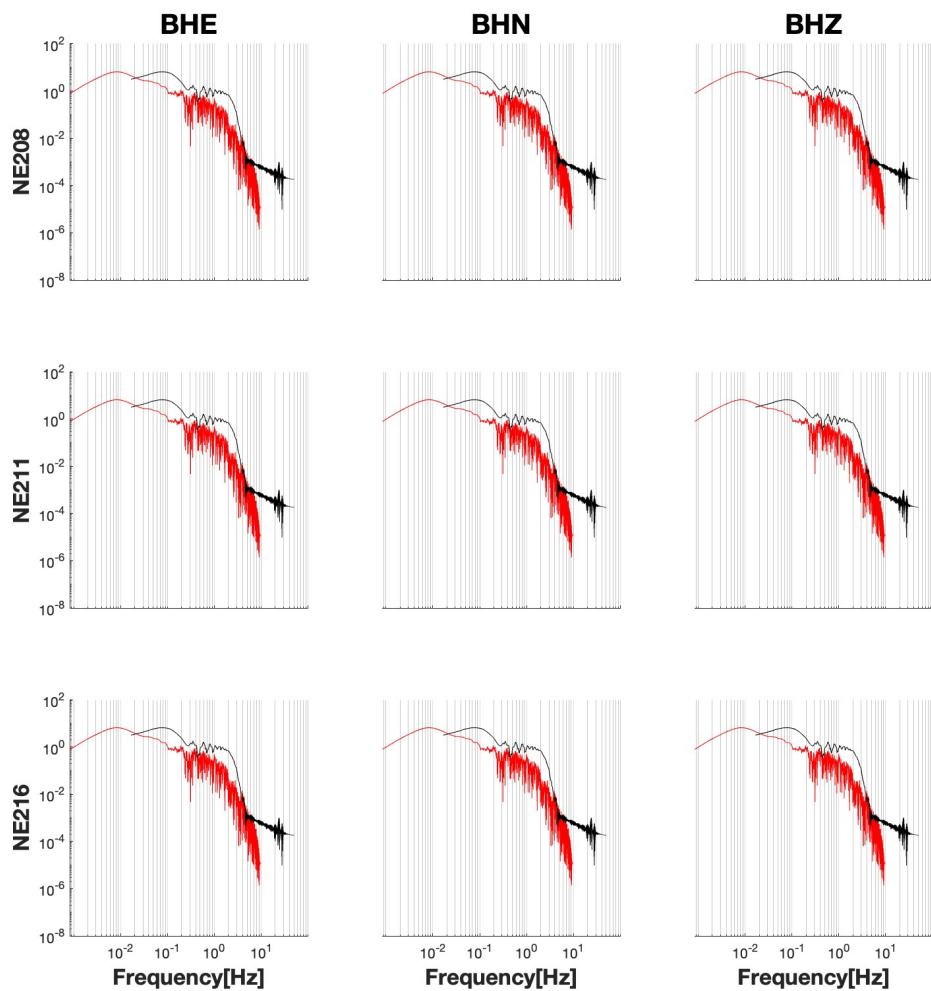


Figure 2.15: Observational and Synthetic spectrum after some scaling, red is obs

2.3.4 Stress distribution: Autocoulomb

Chapter 3

Discussion

3.1 Parameters and Sensitivity

3.1.1 Condition number

Basically, large condition numbers can lead to amplification of small errors.

3.2 Seismic Hazard Assessment for Intraplate regions

3.2.1 Challenges

1. Non-repeatness of IPEs have major implications in assessing the seismic hazard in low tectonic strain intraplate regions
- 2.
- 3.
- 4.

3.3 Comparison of seismicity data and geodetic data

1. InSAR data
- 2.
- 3.
- 4.

Chapter 4

Conclusion and Outlook

4.1 Law

4.1.1 Bath's Law

1. The empirical Bath's law states that the average difference in magnitude between a mainshock and its largest aftershock is 1.2, regardless of the mainshock magnitude.

The mainshock (April 3, 2017) has magnitude at Mw 6.5, and its largest aftershock at Mw 4.6 (April 5, 2017).^[9] The difference is 1.9, a little larger than the average value 1.2.

Appendix A

Supporting Material for Chapter 1

A.0.1 Observations - Rotation of the regional stress field

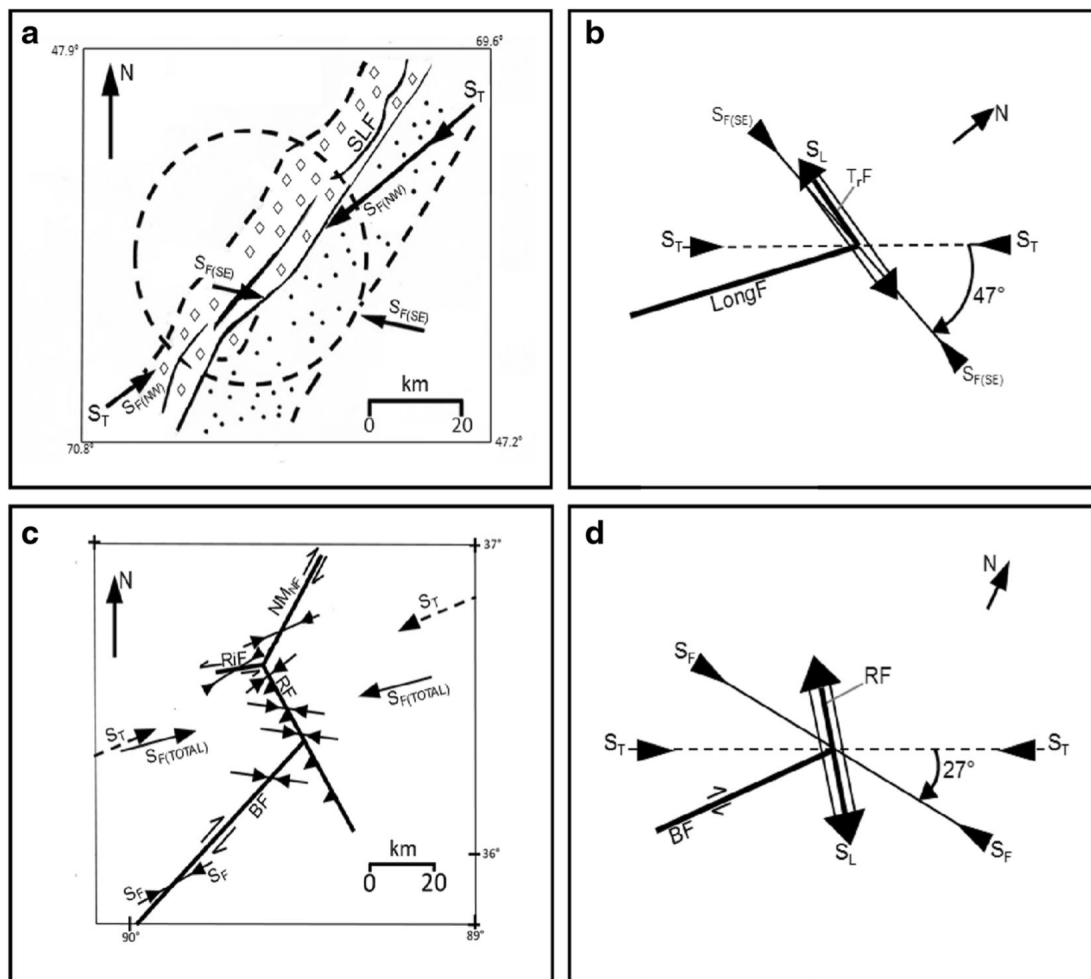


Figure A.1: Rotation of the regional stress field at St. Lawrence and New Madrid [2]

A.0.2 Observations - Large uplifts were observed in the vicinity of faults from InSAR image

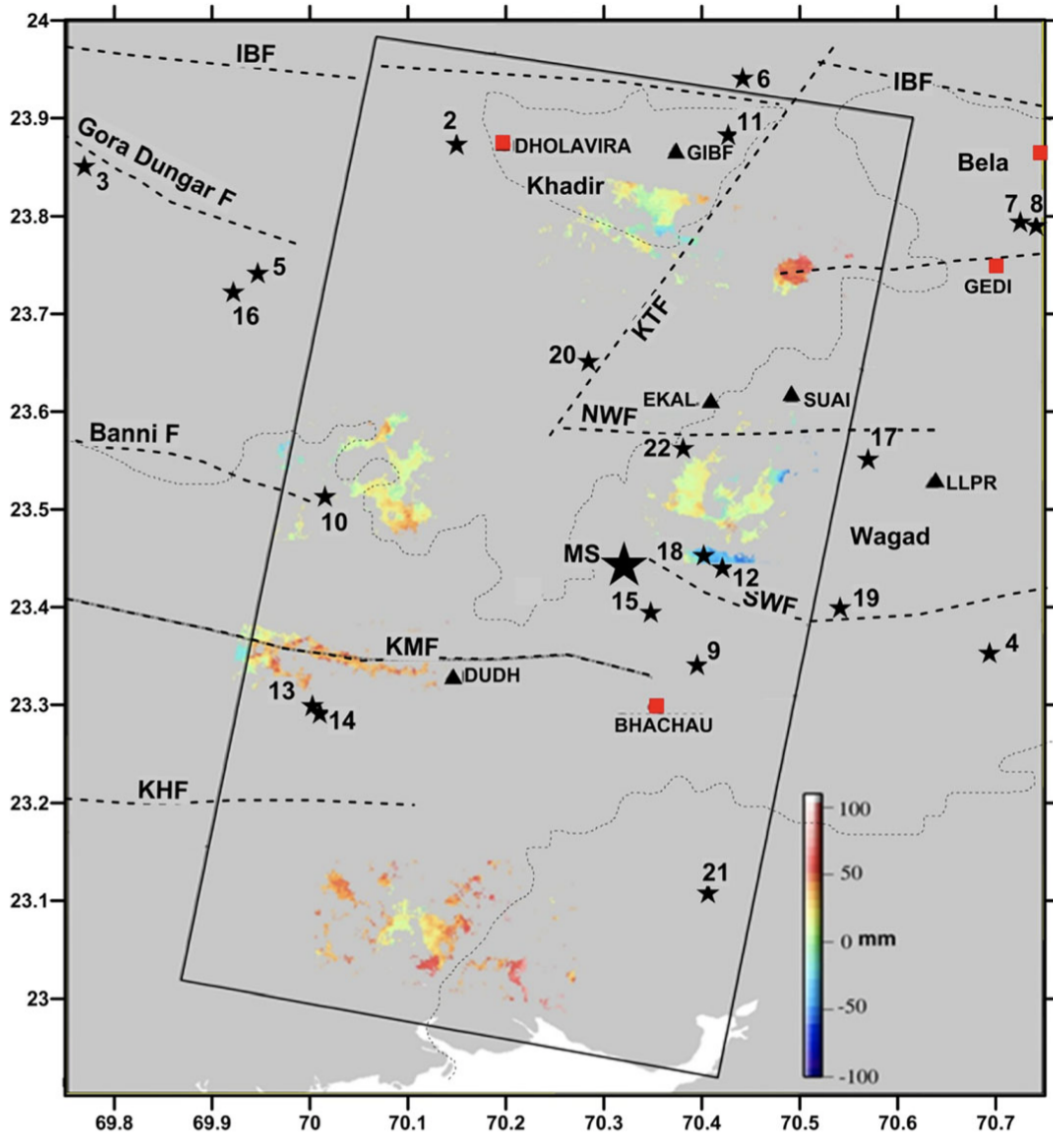


Figure A.2: InSAR showing deviations in LOS in the surrounding area of epicentre of M 7.7 Bhuj earthquake [2]

Large uplifts were observed in the vicinity of faults. Triangles show location of GPS stations. Locations of vertical deformations (colour) are compared with $M \geq 4.0$ aftershocks [2]

Appendix B

Supporting Material for Chapter 2

B.0.1 Resistivity model

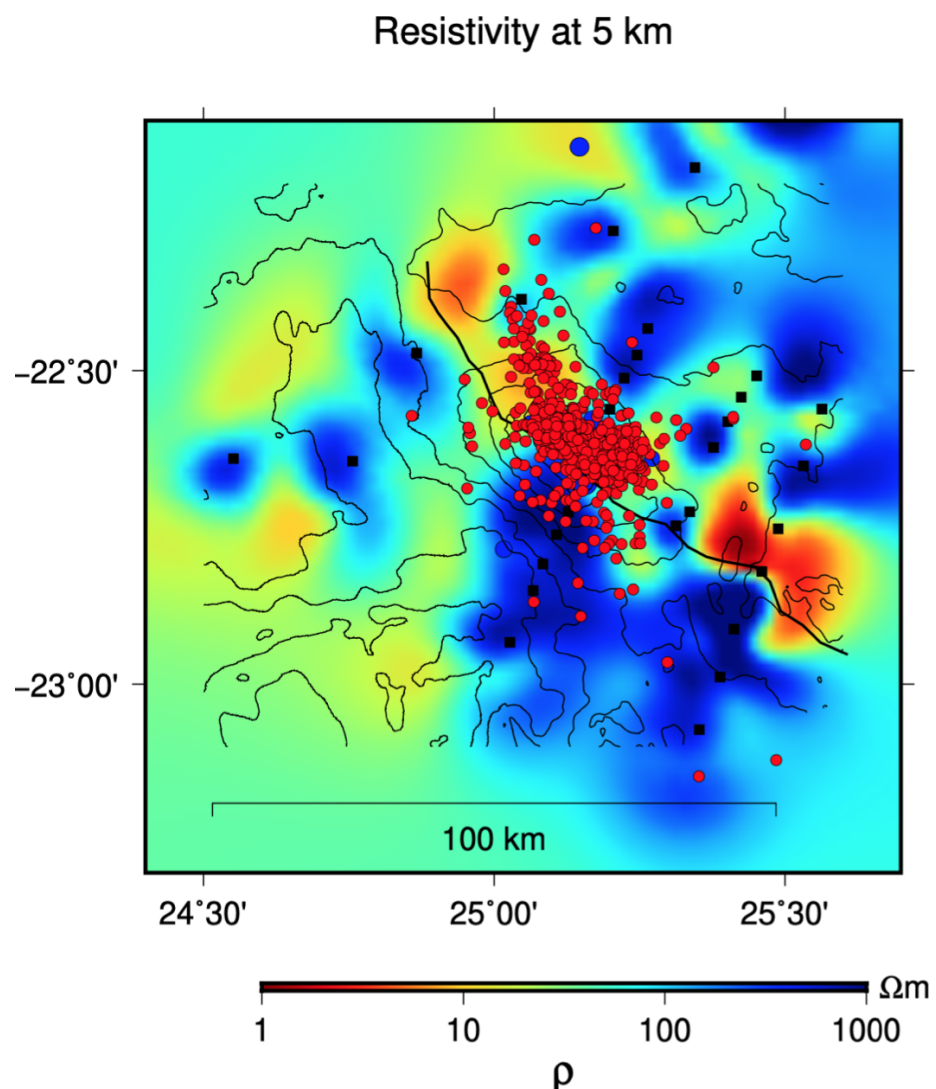


Figure B.1: Estimated fault trace from Moorkamp's resistivity model [3]

Bibliography

- [1] Stephen Hawking. *A brief history of time: from big bang to black holes*. Random House, 2009.
- [2] Pradeep Talwani. On the nature of intraplate earthquakes. *Journal of Seismology*, 21(1):47–68, 2017.
- [3] Max Moorkamp, Stewart Fishwick, Richard J Walker, and Alan G Jones. Geophysical evidence for crustal and mantle weak zones controlling intra-plate seismicity—the 2017 botswana earthquake sequence. *Earth and Planetary Science Letters*, 506:175–183, 2019.
- [4] Thomas Ulrich, Alice-Agnes Gabriel, Jean-Paul Ampuero, and Wenbin Xu. Dynamic viability of the 2016 mw 7.8 kaikōura earthquake cascade on weak crustal faults. *Nature communications*, 10(1):1–16, 2019.
- [5] Folarin Kolawole, Estella A Atekwana, Sean Malloy, D Sarah Stamps, Raphael Grandin, Mohamed G Abdelsalam, Khumo Leseane, and Elisha M Shemang. Aeromagnetic, gravity, and differential interferometric synthetic aperture radar analyses reveal the causative fault of the 3 april 2017 mw 6.5 moiabana, botswana, earthquake. *Geophysical Research Letters*, 44(17):8837–8846, 2017.
- [6] Albano M., Polcari M., Bignami C., Moro M., Saroli M., and Stramondo S. *Did Anthropogenic Activities Trigger the 3 April 2017 Mw 6.5 Botswana Earthquake?* . *Remote Sensing*, 9(10), October 2017. doi: 10.3390/rs9101028.
- [7] Gardonio B., Jolivet R., Calais E., and Leclère H. *The April 2017 Mw 6.5 Botswana Earthquake: An Intraplate Event Triggered by Deep Fluids*. *Geophysical Research Letters*, 45:8886–8896, 2018. doi: 10.1029/2018GL078297.
- [8] Kathryn Materna, Shengji Wei, Xin Wang, Luo Heng, Teng Wang, Weiwen Chen, Rino Salman, and Roland Bürgmann. Source characteristics of the 2017 mw6. 4 moiabana, botswana earthquake, a rare lower-crustal event within an ancient zone of weakness. *Earth and Planetary Science Letters*, 506:348–359, 2019.
- [9] Thifhelimbilu Mulabisana, Mustapha Meghraoui, Vunganai Midzi, Mohamed Saleh, Onkgopotse Ntibinyane, T Kwadiba, Brassnavy Manzunzu, Oarabile Seiphemo, Tebogo Pule, and Ian Saunders. Seismotectonic analysis of the 2017 moiabana earthquake (mw 6.5; botswana), insights from field investigations, aftershock and insar studies. *Journal of African Earth Sciences*, 182:104297, 2021.

Bibliography

- [10] Islam Fadel, Hanneke Paulssen, Mark van der Meijde, Motsamai Kwadiba, Onkgopotse Ntibinyane, Andrew Nyblade, and Raymond Durrheim. Crustal and upper mantle shear wave velocity structure of botswana: The 3 april 2017 central botswana earthquake linked to the east african rift system. *Geophysical research letters*, 47(4):e2019GL085598, 2020.
- [11] Thomas Obermaier. *Mechanisms of intraplate earthquakes: The 2017 Botswana event*. BS Thesis at LMU München, October 2020.
- [12] Kadek Hendrawan Palgunadi, Alice-Agnes Gabriel, Thomas Ulrich, José Ángel López-Comino, and Paul Martin Mai. Dynamic fault interaction during a fluid-injection-induced earthquake: The 2017 m w 5.5 pohang event. *Bulletin of the Seismological Society of America*, 110(5):2328–2349, 2020.

List of Figures

2.1	Two faults model	7
2.2	Two faults model	7
2.3	Mesh visualization	8
2.4	Surface displacement, vertical	11
2.5	Absolute Slip	12
2.8	Rupture Process on the first fault plane	13
2.11	Rupture Process on the second fault plane	14
2.12	Location of the synthetic receivers	15
2.13	Observational and Synthetic seismogram after applied [0.2, 0.6] band pass with order 4 Butterworth filter	16
2.14	Observational and Synthetic seismogram after applied [0.2, 0.6] band pass with order 4 Butterworth filter, cut in 60 seconds	17
2.15	Observational and Synthetic spectrum after some scaling, red is obs	18
A.1	Rotation of the regional stress field at St. Lawrence and New Madrid [2] .	21
A.2	InSAR showing deviations in LOS in the surrounding area of epicentre of M 7.7 Bhuj earthquake [2]	22
B.1	Estimated fault trace from Moorkamp's resistivity model [3]	24

List of Tables

1.1	Purposed fault geometry by various research group	3
2.1	SeisSol Dynamic Rupture Parameters	10

Nomenclature

	Symbols and Abbreviations	Meaning	Note
1	IPEs	Intraplate Earthquakes	
2	LSCs	Local Stress Concentrators	
3	S_v	Vertical stress	
4	S_{Hmax}	Maximum continental horizontal stress	
5	S_F	Final stress	Unified model
6	S_T	Regional stress	Unified model
7	S_L	Local stress	Unified model
8	R	relative prestress ratio	SeisSol
9	SHmax	the direction of maximum horizontal stress	SeisSol

Acknowledgements

I thank L^AT_EX...

Statement of Authorship

With this statement I certify that this master thesis has been composed by myself. Unless otherwise acknowledged in the text, it describes my own work. All references have been quoted and all sources of information have been specifically acknowledged. This thesis has not been accepted in any previous application for a degree.

Selbständigkeitserklärung

Hiermit versichere ich, diese Masterarbeit selbständig und lediglich unter Benutzung der angegebenen Quellen und Hilfsmittel verfasst zu haben. Ich erkläre weiterhin, dass die vorliegende Arbeit noch nicht im Rahmen eines anderen Prüfungsverfahrens eingereicht wurde.